Hindawi
Journal of Nanomaterials
Volume 2022, Article ID 5252918, 11 pages
https://doi.org/10.1155/2022/5252918

Research Article

Heat Transfer Analysis on Carboxymethyl Cellulose Water-Based Cross Hybrid Nanofluid Flow with Entropy Generation

F. Ali,[1] K. Loganathan,[2,3] S. Eswaramoorthi,[4] K. Prabu,[5] A. Zaib,[1] and Dinesh Kumar Chaudhary[6]

[1]*Department of Mathematical Sciences, Federal Urdu University of Arts, Sciences, & Technology, Gulshan-e-Iqbal, Karachi 75300, Pakistan*
[2]*Department of Mathematics and Statistics, Manipal University Jaipur, Jaipur, 303007 Rajasthan, India*
[3]*Research and Development Wing, Live4Research, Tiruppur, 638106 Tamilnadu, India*
[4]*Department of Mathematics, Dr. N.G.P. Arts and Science College, Coimbatore, Tamilnadu, India*
[5]*Department of Physics, Kongu Engineering College, Perundurai, Erode-638060, Tamilnadu, India*
[6]*Department of Physics, Amrit Campus, Tribhuvan University, Kathmandu, Nepal*

Correspondence should be addressed to K. Loganathan; loganathankaruppusamy304@gmail.com and Dinesh Kumar Chaudhary; din.2033@gmail.com

Received 25 December 2021; Revised 15 March 2022; Accepted 2 May 2022; Published 1 June 2022

Academic Editor: Anwar Saeed

The physical phenomena of convective flow of Cross fluid containing carboxymethyl cellulose water over a stretching sheet with convective heating were studied. Cross nanofluid containing Al_2O_3, Cu nanoparticles, and based fluid of CMC water is used. Entropy generation minimization is examined in the current analysis. The system of PDEs is altered into a set of ODEs through suitable conversion. Further, these equations are computed numerically through the MATLAB BVP4c technique. The behavior of governing parameters on the velocity, temperature, entropy generation, and Bejan number is plotted and reported via graphs. It is found that the larger value of unsteady variable reduced the velocity, thermal layer, and entropy production. Surface drag frication of the Al_2O_3 and Cu and Al_2O_3 + Cu is enhanced with the more presence of unsteady parameter. Comparison of current results in a limiting case is obtained with earlier analysis and found an optimum agreement.

1. Introduction

Carboxylmethyl cellulose (CMC) is a water-soluble cellulose derivative [1], and it has many flow properties due to its greater stability and high viscosity. The stability of nanoparticles in CMC escalates the fluid behavior. It is engaged to increase lubricating effects such as polymeric structures [2, 3]. These multifunction aspects of various cellulose derivatives have many industrial and technical applications. To recognize the fluid flow with CMC study, research have been studied [4–6]. Saqib et al. [7] described the natural convective flow of CMC with carbon nanotube using a fractional derivative approach. The effect of slip velocity and non-Newtonian nanofluid contained with 0.5% wt CMC water was discussed by Rahmati et al. [8]. Akinpelu et al. [9] explored the thermophysical metal properties in CMC. MHD flow of Casson nanofluid under heat transfer in CMC over a solid sphere was developed by Alwawi et al. [10].

Nanotechnology has been progressively more fascinated by the researchers because of their efficiency in several industrial processes such as microelectronic, oil emulsion, and molecular emulsion. Nanotechnology has the ability in suspending nanoscale particles $(1 \le 100\text{nm})$ in ordinary fluids, like ethylene glycol, oil, and water. The origin of nanotechnology was initiated by Choi and Eastman [11] in 1995. After, Buongiorno [12] developed a mathematical model of heat transfer with the addition of Brownian motion and thermophoresis effects. Tiwari and Das [13] investigated to examine the solid volume fraction in nanofluids. Devi and Devi [14] reported the numerical simulation of hybrid

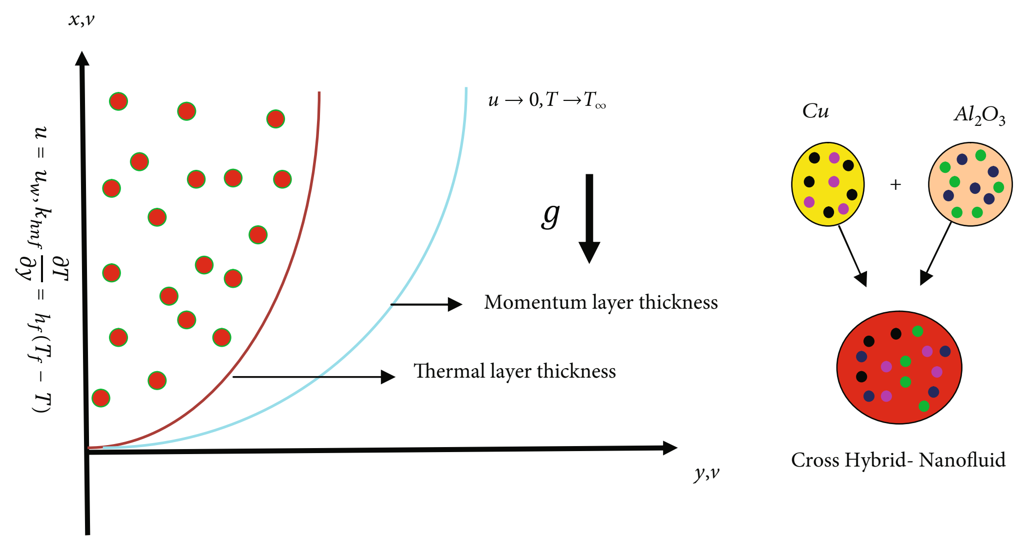

Figure 1: Geometry of problem.

nanofluid over a porous surface with suction. Afridi et al. [15] carried out the heat transfer analysis in hybrid nanofluid under fraction heating. The effect of second law analysis with hybrid nanofluid and viscous dissipation due to rotating disk was scrutinized by Farooq et al. [16]. Devi et al. [17, 18] revealed the heat transfer of hybrid nanofluid flow with two different base fluids. Gorla et al. [19] addressed the impact of heat sink/source in the hybrid nanofluid past the permeable surface. Chamkha et al. [20] analyzed the time-dependent flow of mixed convective hybrid nanofluid over half cavity. More recently, Zainal et al. [21] disclosed the unsteady 3-D MHD stagnation point flow of hybrid nanofluid using stability analysis. Few more cutting edge research reports are seen in Refs. [22–28].

The study of entropy optimization has broad features in the thermal engineering process such as heat pump, heat engine, solar power, and refrigerator. The improvement of the thermal system is enhanced due to the entropy production. The Bejan number [29] is a dimensionless quantity that represents overall entropy generation ratio of heat transmission and total entropy generation. Khana et al. [30] discussed the computational analysis of hybrid nanofluid with entropy generation due to rotating disk between parallel plates. Dawar et al. [31] surveyed the heat transfer analysis through SWCNTs/MWCNTs in entropy generation and activation energy over a moving wedge. The numerical study of second law analysis of nanofluid due to an inclined surface was discussed by Butt et al. [32]. Heat transfer in MHD third-grade nanofluid with convective condition and entropy generation over a stretching surface was encountered by Rashidi et al. [33]. The investigation of entropy production for the magnetic field, thermal radiation, and porous medium was reported by Makinde and Eegunjobi [34]. The impact of entropy generation on two permeable stretched surfaces was inspected by Khan et al. [35]. Afridi et al. [36] described the hybrid nanofluid flow over a thin needle with entropy generation. Reddy et al. [37] studied the entropy generation on Williamson nanofluid with thermal radiation and internal heat source over the lubricated surface.

The behavior of non-Newtonian fluid models, like second grade, power law, and Williamson, was investigated by many researchers in the past few years due to their vital role in engineering and industrial applications. However, these models cannot be recognized to analyze the behavior of fluid at higher and lower shear rates. To illustrate the behavior of fluid at a very low and high shear rate, the Cross fluid model has been introduced by Cross [38]. The Cross fluid model has optimum potential to trounce the challenges that are overlooked while the shear rate is highly accelerated or depreciated. Few recent developments under this direction are collected in [39, 40]. The effect of heat source/sink on Cross fluid with thermal radiation was studied by Nazeer et al. [41]. Sabir et al. [42] scrutinized the heat transfer phenomena through radiation and activation energy over an inclined sheet. Yao et al. [43] investigated the magnetic dipole effect for Cross fluid through spectroscopy. Khan et al. [44] interpreted the effect of thermal radiative and activation energy on Cross fluid near the stagnation point. Reddy and Ali [45] constructed the MHD Cross nanofluid under Cattaneo-Christov double diffusion theory over a vertical stretching sheet.

The abovementioned studies reveal the focus on the heat transport analysis of a CMC-nanofluid, but no authors examined the CMC-hybrid nanofluid in the presence of unsteady Cross fluid with the effect of mixed convection. So, the authors attempted to investigate the heat transfer analysis of CMC-based Cross hybrid nanofluid with convective heating. The system of PDEs is transformed into ODEs through the suitable transformation, and these ODEs are tackled through BVP4c for numerical solution. The entropy analysis is implemented in the present study. This combination is more useful in thermal and aerospace engineering.

2. Mathematical Formulation

Let us consider the unsteady incompressible mixed convective flow of Cross hybrid nanofluid over a stretching sheet with surface heating. Moreover, Cartesian coordinates have

Table 1: Thermophysical properties.

Physical properties	Specific heat capacity	Density	Thermal conductivity	Coefficient of thermal expansion
CMC-water (<0.4%)	4179	997.1	0.613	21
Al_2O_3	765	3970	40	0.85
Cu	531.8	6320	76.5	1.80
Dynamic viscosity	Π_1	$\frac{\mu_{\mathrm{hnf}}}{\mu_f}=\frac{1}{(1-\varphi_1-\varphi_2)^{2.5}}$		
Density	Π_2	$\frac{\rho_{\mathrm{hnf}}}{\rho_f}=(1-\varphi_2)\left[(1-\varphi_1)+\frac{\varphi_1\rho_{1s}}{\rho_f}\right]+\frac{\varphi_2\rho_{2s}}{\rho_f}$		
Thermal expansion	Π_3	$\frac{(\rho\beta_T)_{\mathrm{hnf}}}{(\rho\beta_T)_f}=(1-\varphi_2)\left[(1-\varphi_1)+\frac{\varphi_1(\rho\beta_T)_{1s}}{(\rho\beta_T)_f}\right]+\frac{\varphi_2(\rho\beta_T)_{2s}}{(\rho\beta_T)_f}$		
Heat capacity	Π_4	$\frac{(\rho c_p)_{\mathrm{hnf}}}{(\rho c_p)_f}=(1-\varphi_2)\left[(1-\varphi_1)+\frac{\varphi_1(\rho c_p)_{1s}}{(\rho c_p)_f}\right]+\frac{\varphi_2(\rho c_p)_{2s}}{(\rho c_p)_f}$		
Thermal conductivity	Π_5	$\frac{k_{\mathrm{hnf}}}{k_f}=\frac{k_{2s}+2k_f-2\varphi_2(k_f-k_{2s})}{k_{2s}+2k_f+\varphi_2(k_f-k_{2s})}\times(k_{\mathrm{nf}})\,k_{\mathrm{nf}}=\frac{k_{1s}+2k_f-2\varphi_1(k_f-k_{1s})}{k_{1s}+2k_f+\varphi_1(k_f-k_{1s})}$		

been taken in the x-axis along the sheet, and y-axis is perpendicular to surface as seen in Figure 1. The radiation can only travel a distance within thick nanofluid; so, the Rosseland approximation is considered into account for radiative heat transfer.

Under the above assumptions, the flow model can be extract as follows:

$$\frac{\partial u}{\partial x}+\frac{\partial v}{\partial y}=0, \tag{1}$$

$$\frac{\partial u}{\partial t}+u\frac{\partial u}{\partial x}+v\frac{\partial u}{\partial y}=\nu_{\mathrm{hnf}}\frac{\partial}{\partial y}\left(\frac{\partial u/\partial y}{1+\Gamma(\partial u/\partial y)^n}\right)+\frac{g}{\rho_{\mathrm{hnf}}}(\rho\beta_T)_{\mathrm{hnf}}(T-T_\infty)=0, \tag{2}$$

$$\frac{\partial T}{\partial t}+u\frac{\partial T}{\partial x}+v\frac{\partial T}{\partial y}=\frac{k_{\mathrm{hnf}}}{(\rho C_p)_{\mathrm{hnf}}}\frac{\partial^2 T}{\partial y^2}-\frac{1}{(\rho C_p)_{\mathrm{hnf}}}\frac{\partial q_r}{\partial y}. \tag{3}$$

The boundary constraints are applied as follows:

$$u=u_w(x,t),\, v=0,-k_{\mathrm{hnf}}\frac{\partial T}{\partial \widehat{y}}=h_f\left(T_f-T_\infty\right)\text{ at } y=0,$$
$$u=u(x,t)=0,\, T\longrightarrow T_\infty \text{ as } y\longrightarrow\infty. \tag{4}$$

Here, u, v, μ_{hnf}, ρ_{hnf}, k_{hnf}, $(\rho C_P)_{\mathrm{hnf}}$, and q_r are horizontal velocity and vertical velocity, viscosity, density, thermal conductivity, specific heat capacity, and thermal radiative for hybridnanoflud, respectively. h_f is the heat transfer coefficient.

Table 2: Validation of current results of $-\theta'(0)$ with Wakif [48] against Pr.

Pr	Wakif [48]	Current analysis
0.7	0.453916157	0.456051210134421
2.0	0.911357683	0.911321374513764
7.0	1.895403258	1.895381882154913
20	3.353904143	3.353886925689145
70	6.462199531	6.462184407558267

Table 3: Comparing of $f''(0)$ for unsteady parameter δ when $n=\mathrm{We}=\lambda=0$.

δ	Ali and Zaib [49]	Current results
0.8	-1.261211	-1.260691
1.2	-1.377625	-1.377710

2.1. Suitable Transformation for Unsteady Flow. It is relevant to use the following appropriate transformation:

$$\eta=y\sqrt{\frac{a}{\upsilon_f(1-\chi t)}},\, u=\frac{ax}{(1-\chi t)},f'(\eta),$$
$$v=\sqrt{\frac{a\upsilon_f}{(1-\chi t)}}f(\eta),\theta(\eta)=\frac{T-T_\infty}{T_f-T_\infty}. \tag{5}$$

Using the suitable transformation described in Eq. (5), to Eq. (2), Eq. (3) altered into the following ordinary differential equations with respect to parameter η:

$$\Pi_1\left[\left(1+(1-n)\left(\mathrm{We}f''\right)^n\right)f'''\right]+\Pi_2\left[ff''-\delta\left(f'+\frac{\eta}{2}f''\right)-\left(f'\right)^2\right]\cdot\left(1+\left(\mathrm{We}f''\right)^n\right)^2+\Pi_3\lambda\theta\left(1+\left(\mathrm{We}f''\right)^n\right)^2=0, \tag{6}$$

Table 4: Numerical outcomes of value of skin friction coefficient and local Nusselt number.

We	λ	δ	Bi	Pr	Rd	$Re_x^{1/2}C_f$ Cu	Al_2O_3	$Cu + Al_2O_3$
1.5	0.9	0.1	0.2	6.2	0.5	2.7247	2.3915	5.1162
2.0			0.3			1.1420	1.1102	2.2522
2.5			0.4			0.5355	0.5097	1.0452
1.0	1.4	0.2	0.2	6.8	0.7	2.7469	2.4140	5.1609
1.1			0.3			1.1550	1.1226	2.2776
1.2			0.4			0.5460	0.5102	1.0562
1.0	1.5	0.3	0.2	7.2	0.9	2.7480	2.4339	5.1819
1.1			0.3			1.1643	1.1361	2.3004
1.2			0.4			0.5507	0.5222	1.0729

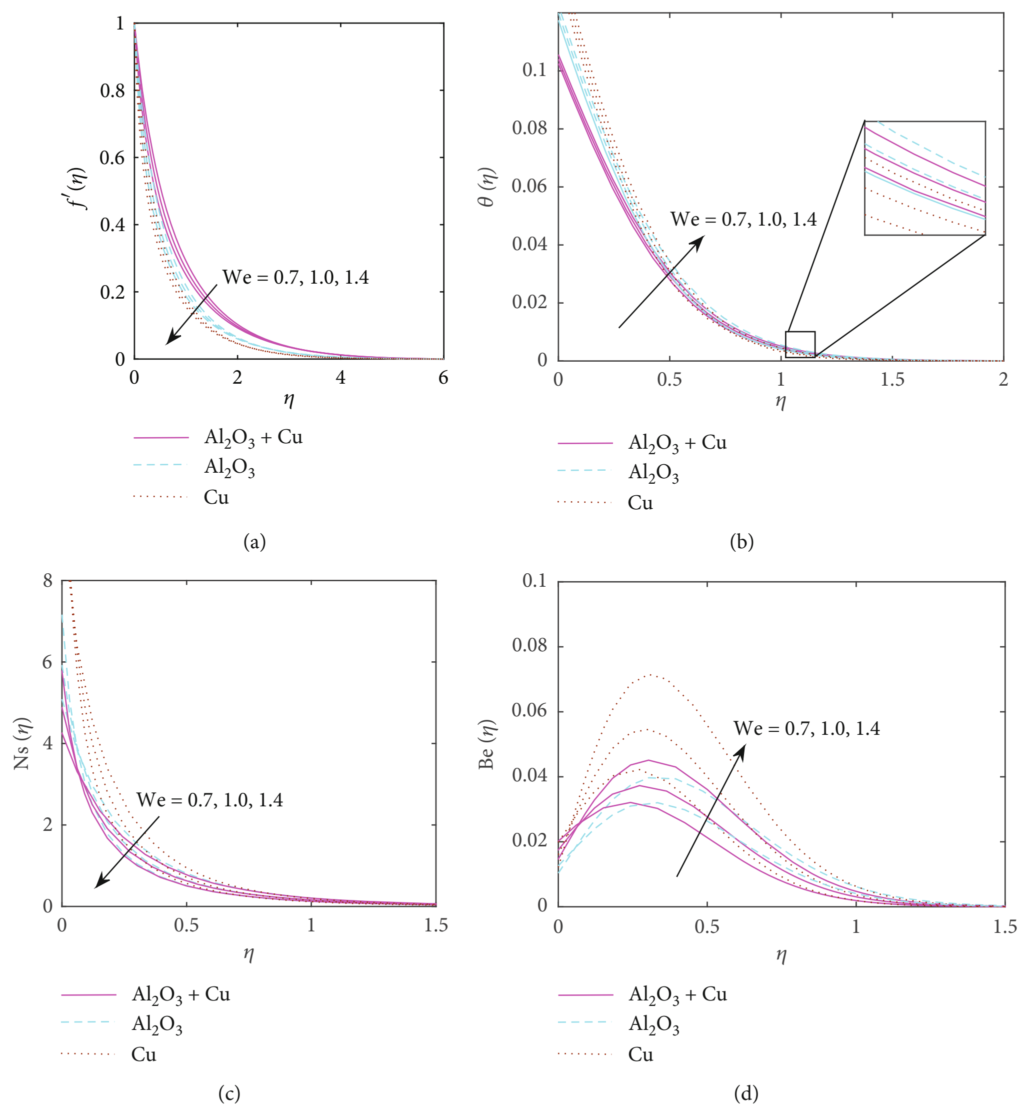

Figure 2: (a)–(d) $f'(\eta), \theta(\eta), \mathrm{Ns}(\eta), \mathrm{Be}(\eta)$ versus We.

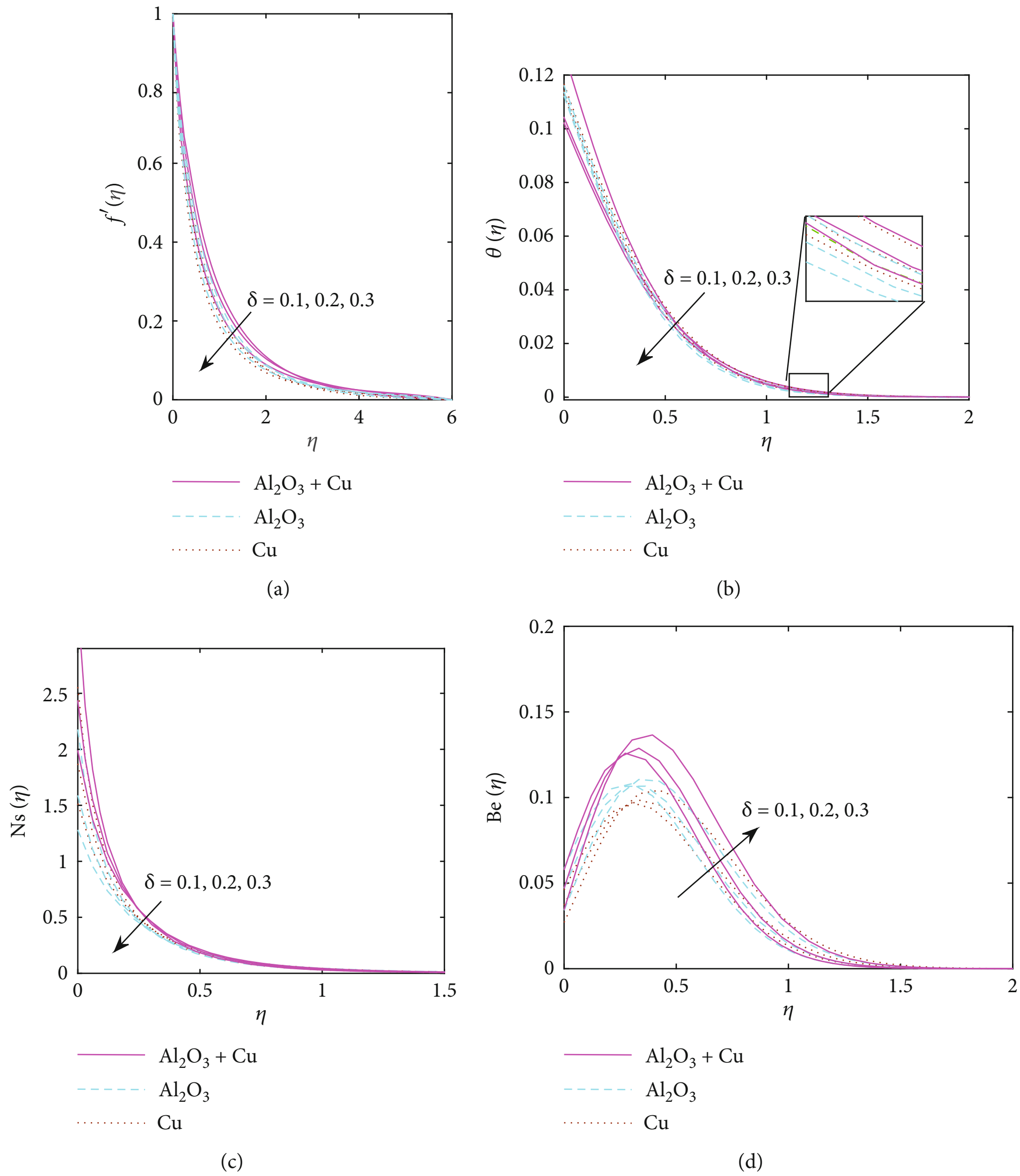

Figure 3: (a)–(d) $f'(\eta), \theta(\eta), \mathrm{Ns}(\eta), \mathrm{Be}(\eta)$ versus δ.

$$\theta''(1+\Pi_4 \mathrm{Rd}) - \frac{\Pi_3}{\Pi_4}\frac{\eta}{2}\delta \mathrm{Pr}\theta' + \mathrm{Pr}\Pi_5 f\theta' = 0. \tag{7}$$

The transformation boundary conditions are stated as follows:

$$f(0)=0, f'(0)=1, \Pi_4\theta'(0) = -\mathrm{Bi}(1-\theta(0)), f'(\infty) = 0, \theta(\infty)=0. \tag{8}$$

Nondimensionless governing variables are Weissenberg number $\mathrm{We}(=\Gamma ax\sqrt{a/v})$, unsteady parameter $\delta(=c/a)$, mixed convection $\lambda(=\mathrm{Gr}_x/\mathrm{Re}_x^2)$, Prandtl number $\mathrm{Pr}(=\mu_f (c_p)_x/k_f)$, radiation parameter $(\mathrm{Rd}=(16\sigma^* T_\infty^3)/(\mathrm{kk}^*))$, the skin friction coefficient C_f, and the local Nusselt number which are presented by

$$C_f = \left(\frac{\tau_w}{\rho_f u_w^2}\right), \mathrm{Nu} = \left(\frac{x q_w}{k_f (T_f - T_\infty)}\right). \tag{9}$$

Wall shear stress and heat flux are as follows:

$$\tau_w = \mu_{\mathrm{hnf}}\left(\frac{\partial u}{\partial y}\right)_{y=0}, q_w = -k_{\mathrm{hnf}}\left(\frac{\partial T}{\partial y}\right)_{y=0}. \tag{10}$$

In view of Eqs. (5) and (10), we get

$$\mathrm{Re}_x^{1/2} C_f = \Pi_1 \left(\frac{f''(0)}{1+\left(\mathrm{We} f''(0)\right)^n}\right)_{y=0}, \mathrm{Re}_x^{-1/2}\mathrm{Nu}_x = \left(\Pi_5 (1+\mathrm{Rd})\theta'(0)\right)_{y=0}. \tag{11}$$

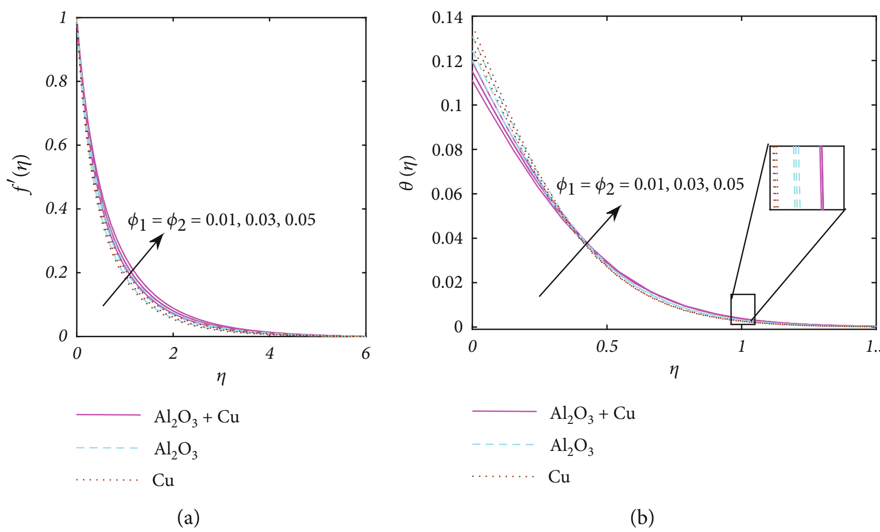

Figure 4: (a, b) $f'(\eta), \theta(\eta)$ versus $\phi_1, \phi_2.$

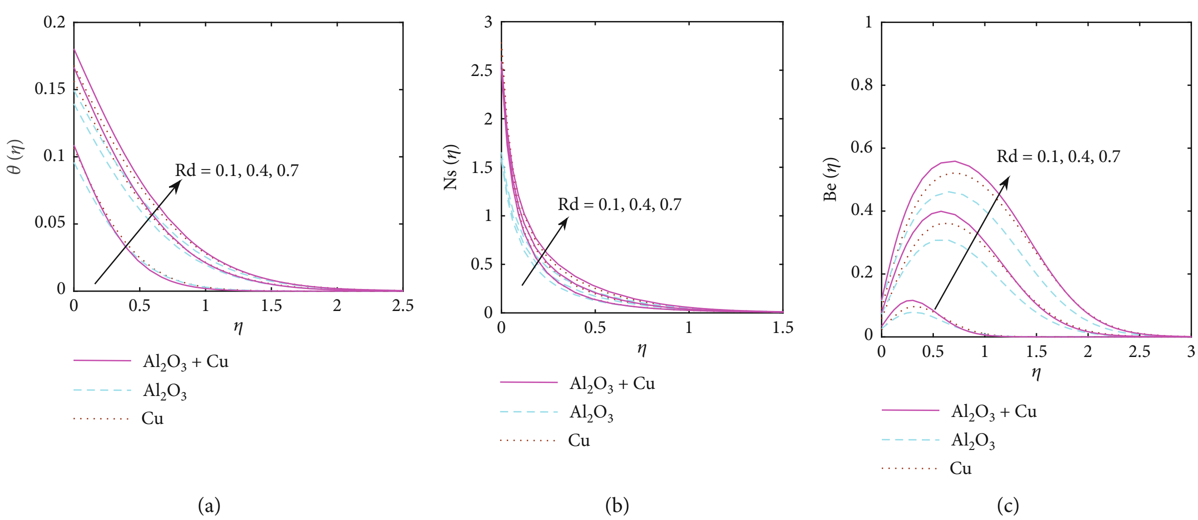

Figure 5: (a)–(c) $\theta(\eta)$, $Ns(\eta)$, $Be(\eta)$ versus Rd.

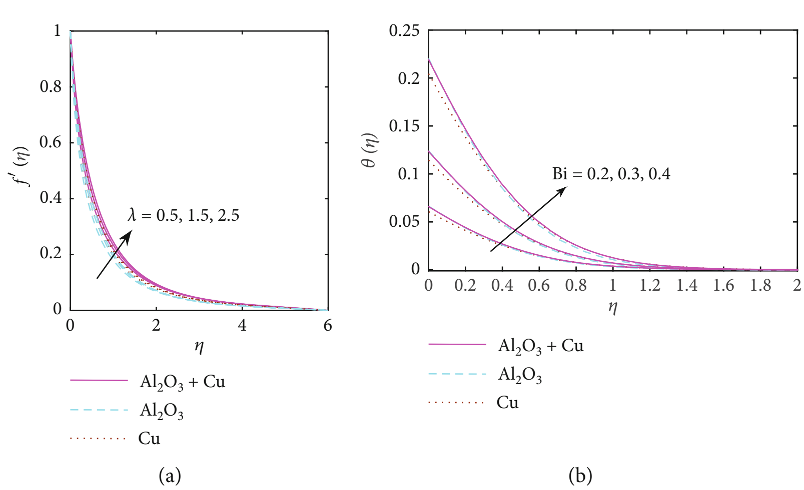

Figure 6: (a, b) $f'(\eta)$ and $\theta(\eta)$ versus λ and Bi.

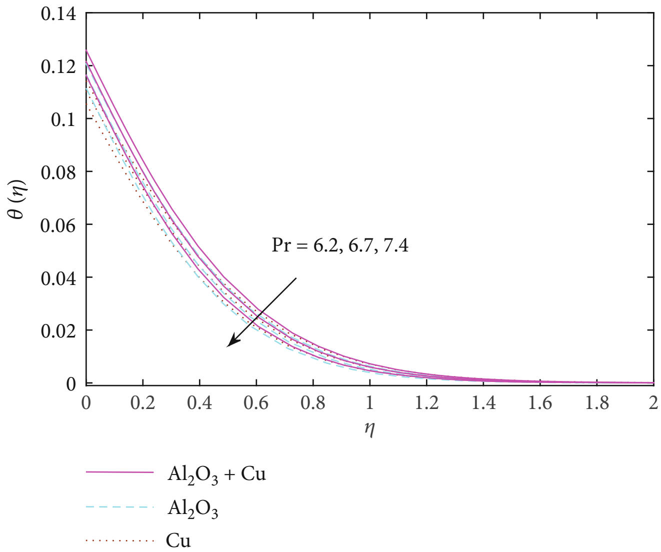

Figure 7: $\theta(\eta)$ versus Pr.

3. Entropy Generation

The appearance of entropy production for Cross hybrid nanoliquid over a stretching sheet is defined as [46, 47]:

$$E_G = \frac{k_f}{T_\infty^2}\left[\frac{k_{\text{hnf}}}{k_f} + \frac{16\sigma * T_\infty^2}{3k_f k *}\left(\frac{\partial T}{\partial y}\right)^2\right] + \mu_{\text{hnf}}\frac{1}{T_\infty}\left(\frac{\partial u}{\partial y}\right)^2\left(\frac{1}{1+\Gamma(\partial u/\partial y)^n}\right). \quad (12)$$

The characteristics entropy generation is described below:

$$E_0''' = \frac{\mathrm{k}_{\text{hnf}}\left(T_f - T_\infty\right)}{x\mathrm{T}_\infty^2}. \quad (13)$$

The dimensionless form of entropy generation is $Ns = N_h + N_v$.

$N_h = \Pi_5[1+\mathrm{Rd}](\theta')^2$ is the entropy generation due to heat transfer, and $N_v = \Pi_4[1+(1/(\mathrm{We}f'')^n)]f''^2$ is the entropy generation due to fluid friction.

$$Ns = \frac{E_G}{E_0'''} = \Pi_5[1+\mathrm{Rd}]\left(\theta'\right)^2 + \mathrm{Br}\Pi_4\left[1+\frac{1}{\left(\mathrm{W}ef''\right)^n}\right]f''^2. \quad (14)$$

The Bejan number is defined by

$$\mathrm{Be} = \frac{\Pi_5[1+\mathrm{Rd}]\left(\theta'\right)^2}{\Pi_5[1+\mathrm{Rd}]\left(\theta'\right)^2 + +\mathrm{Br}\Pi_4\left[1+\left(1/\left(\mathrm{We}f''\right)^n\right)\right]f''^2}. \quad (15)$$

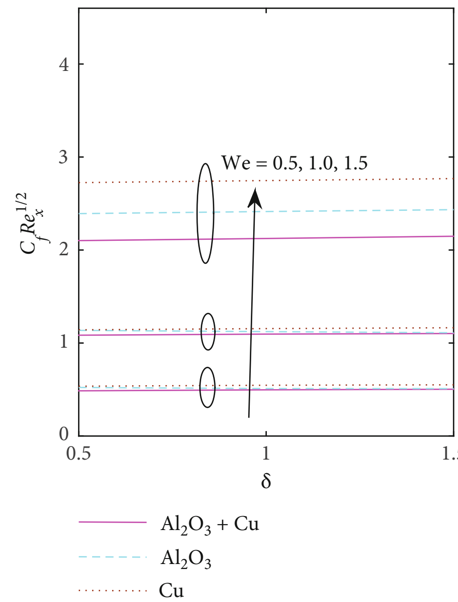

Figure 8: The influence of We and δ on $C_f\ \mathrm{Re}_x^{1/2}$.

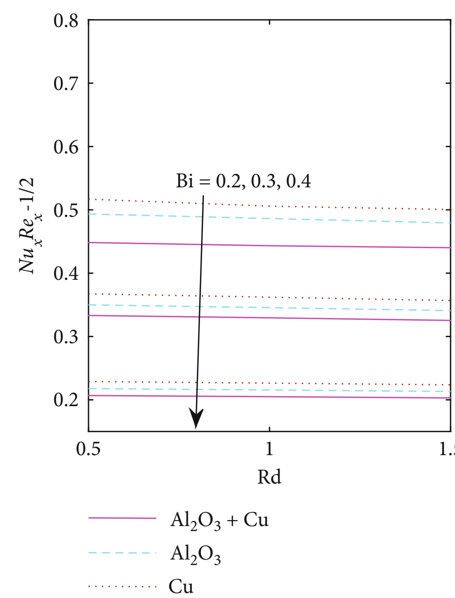

Figure 9: The influence of Rd and Bi on $\mathrm{Nu}_x\ \mathrm{Re}_x^{-1/2}$.

4. Numerical Investigation

The set of an altered system of highly nonlinear ODE's equations (6)–(7) with subject to the boundary condition (8) has been numerically computed with aid of the BVP4c method. For this purpose, first, we converted the higher order derivative into first order.

$$f = \Lambda_1, f' = \Lambda_2, f'' = \Lambda_3, f''' = \Lambda_3', \theta = \Lambda_4, \theta' = \Lambda_5, \theta'' = \Lambda_5', \quad (16)$$

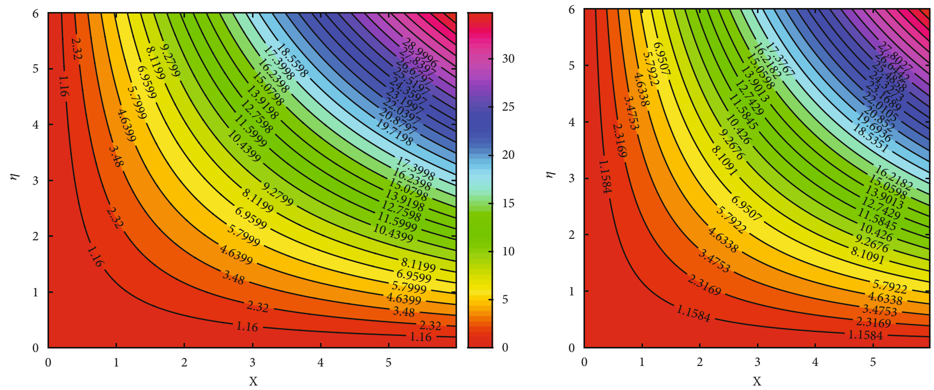

(a) (b)

FIGURE 10: Stream line pattern for various values $\phi_1 = 0, \phi_2 = 0$ and $\phi_1 = 0.02, \phi_2 = 0$.

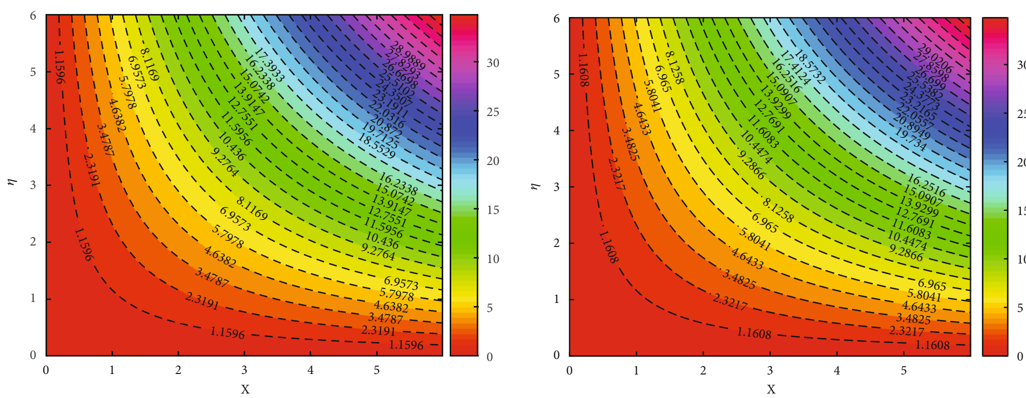

(a) (b)

FIGURE 11: Stream line pattern for (a) unsteady flow and (b) steady flow.

$$\Lambda_3' = \frac{-\Pi_2\left[\Lambda_1\Lambda_3 - \delta(\Lambda_2 + (\eta/2)\Lambda_3) - (\Lambda_2)^2\right]\left\{1 + (\mathrm{We}\Lambda_3)^n\right\}^2 - \Pi_3\lambda\Lambda_4\left\{1 + (\mathrm{We}\Lambda_3)^n\right\}^2}{\Pi_1\left[(1 + (1-n)(\mathrm{We}\Lambda_3)^n)\right]}, \tag{17}$$

$$\theta''\left(1 + \Pi_4\frac{4}{3}\mathrm{Rd}\right) - \frac{\eta}{2}\delta\frac{\Pi_3}{\Pi_4}\mathrm{Pr}\theta' + \mathrm{Pr}\Pi_5 f\theta' = 0,$$
$$\Lambda_5' = \frac{-\mathrm{Pr}\Pi_5\Lambda_1\Lambda_5 + (\eta/2)\delta(\Pi_3/\Pi_4)\mathrm{Pr}\Lambda_4}{(1 + \Pi_4\mathrm{Rd})} \tag{18}$$

Converted boundary conditions are as follows:

$$\Lambda_1(0) = 0, \Lambda_2(0) = 1, \Lambda_5(0) = -\mathrm{Bi}(1 - \Lambda_4(0)), \Lambda_2(\infty) = 0, \Lambda_4(\infty) = 0. \tag{19}$$

The iterative process has been used, and the accuracy of the solution is obtained to 10^{-6}.

5. Result and Discussion

In this segment, we examine the variations of $f'(\eta)$, $\theta(\eta)$, Ns(η), and Be(η) for different flow variables, such as Weissenberg number (We), Biot number (Bi), Prandtl number (Pr), thermal radiation (Rd), nanoparticle volume fraction (ϕ_1, ϕ_2), and mixed convection parameter (λ). For performing graphical study, single variable varies, whereas all the physical variables were kept in constant values such as $\mathrm{We} = 0.5$, $n = 0.4$, $\mathrm{Bi} = -0.3$, $\lambda = 1.0$, $\mathrm{Pr} = 6.2$, $\delta = 0.3$, $\mathrm{Rd} = 1.7$. Table 1 demonstrates the thermophysical properties of Cu, Al_2O_3, and Cu+Al_2O_3. Tables 2 and 3 show the comparison outcome of $-\theta(0)$ against Pr and $f''(0)$ against δ with the limiting case $n = \mathrm{We} = \lambda = 0$. From these tables, it is found that our computations are optimum one. Table 4 shows the impact of We,λ, δ, Bi, Pr, and Rd on skin friction coefficient for Cu, Al_2O_3, and Cu+Al_2O_3.

Figures 2(a)–2(d) display the fluctuation of Weissenberg (We) on velocity distribution $f'(\eta)$, temperature field $\theta(\eta)$, entropy production Ns(η), and Bejan number Be(η) for nanofluids (Cu&Al_2O_3) and hybrid nanofluid (Cu + Al_2O_3). The fluid velocity and entropy generation reduce when We augments. However, fluid temperature and Bejan number enhance when enhancing the quantity of We. Physically, the Weissenberg number means shear rate time which helps to rise the fluid thickness, and this causes to depreciate fluid velocity. The variations of δ on $f'(\eta)$, $\theta(\eta)$, Ns(η), and Be(η) are illustrated in Figures 3(a)–3(d) for nanofluids and hybrid nanofluid. It is seen from these figures that the fluid velocity, fluid temperature, and entropy production decline when increasing the magnitude of δ, and Bejan number raises when rising the values of δ. Figures 4(a) and 4(b)present the consequences of ϕ_1 and ϕ_2 on $f'(\eta)$ and $\theta(\eta)$ for nanofluids and hybrid nanofluid for nanofluids and hybrid nanofluid. It is seen that the fluid velocity and fluid temperature upsurge when mounting the quantity of ϕ_1 and ϕ_2. The impact of radiation on $\theta(\eta)$, $\mathrm{Ns}(\eta)$, and $\mathrm{Be}(\eta)$ was portrayed in Figures 5(a)–5(c) for nanofluids and hybrid nanofluid. It is concluded that the fluid temperature, entropy production, and Bejan number are increasing function of radiation parameter. Physically radiation parameter enhances the rate energy transport to the fluid and thereby enriching the fluid temperature and thicken the thermal boundary layer. Figures 6(a) and 6(b) provide the changes of $f'(\eta)$ on λ and $\theta(\eta)$ on Bi for nanofluids and hybrid nanofluid. It is detected that the momentum boundary layer thickness escalates when enriching the λ values, see Figure 6(a). The fluid temperature raises when raising the Biot number, see Figure 6(b). Physically, Biot number leads to enrich the heat transfer coefficient, this leads to enhance the fluid thermal state, and this causes to improve the fluid temperature and thicker the thermal boundary layer thickness. Figure 7 displays the effect of Pr on $\theta(\eta)$ for nanofluids and hybrid nanofluid. It is found that the fluid temperature and its associated boundary layer thickness downturn when strengthening the Prandtl number.

Figure 8 shows the influence of δ and We on skin friction coefficient for nanofluids and hybrid nanofluid. It is proved from this figure that the skin friction coefficient enriches when strengthening the We values, and it is almost fixed when changing the δ values. Further, the skin friction coefficient is low in hybrid nanofluid than the nanofluids case. The local Nusselt number for various values of Rd and Bi for nanofluids and hybrid nanofluid is plotted in Figure 9. It is seen that the heat transfer gradient depresses when enriching the Rd and Bi for all cases. In addition, the less local Nusselt number is attained in hybrid nanofluid than the nanofluids case. Finally, Figures 10 and 11 present the streamline pattern for numerous values of nanoparticle volume fraction, Stedy and unstedy flows.

6. Final Remarks

The two-dimensional mixed convection flow of Cross fluid is based on CMC-water with nanoparticles Cu and Al_2O_3 with thermal radiation over a stretching sheet. The second law analysis has been made. The physical model is computed via the MATLAB BVP4c function. The numerical and graphical results for flow and energy transfer are produced for diverse values of dimensionless variables. Moreover, skin friction and Nusselt number have been computed. The main findings of this work are as follows:

(i) Momentum boundary layer thickness of Cu, Al_2O_3, and Cu+Al_2O_3 reduces as the Weissenberg number We is enhanced.

(ii) The temperature profile Cu, Al_2O_3, and Cu+Al_2O_3 is reduced for both δ and We.

(iii) Entropy generation and Bejan number of Cu, Al_2O_3, and Cu+Al_2O_3 are quite similar trends for We and δ.

(iv) Temperature distribution, entropy generation, and Bejan number Cu, Al_2O_3, and Cu+Al_2O_3 are enhanced as increases the value of thermal radiation Rd.

(v) Both Biot number and mixed convection are enhanced for temperature and velocity distribution of Cu, Al_2O_3, and Cu+Al_2O_3.

(vi) The drag friction and Nusselt number have an increasing effect for nanofluid and hybrid nanofluid.

Nomenclature

a: Stretching rate
t: Time
λ: Mixed convection parameter
k_{nf}: Effective thermal conductivity
ρ_{f}: Reference density of fluid
ρ_{s}: Reference density of solid
Pr: Prandtl number
Bi: Biot number
Be: Bejan number
Ns: Total entropy generation
μ_f: Viscosity of fluid
We: Weissenberg number
δ: Unsteady parameter
n: Power-law index
k: Thermal conductivity of base fluid
u: Velocity along the x-axis
v: Velocity along the y-axis
ρ_{nf}: Density of fluid
μ_{nf}: Effective viscosity of nanofluid
Nu_x: Nusselt number
k_f: Thermal conductivity of fluid
k_s: Thermal conductivity of solid
Re_x: Local Reynolds number
T: Fluid temperature
T_f: Temperature of the hot fluid

Abbreviations

Cu: Copper
PDE: Partial differential equations
ODE: Ordinary differential equations
CMC: Carboxylmethyl cellulose.

Data Availability

The raw data supporting the conclusions of this article will be made available by the corresponding author without undue reservation.

Conflicts of Interest

The authors declare that they have no conflicts of interest.

Authors' Contributions

All authors listed have made a substantial, direct, and intellectual contribution to the work and approved it for publication.

References

[1] I. H. Mondal, *Carboxymethyl cellulose: synthesis and characterization*, Nova Science Publishers, Hauppauge, NY, USA, 2019.

[2] A. Benchabane and K. Bekkour, "Rheological properties of carboxymethyl cellulose (CMC) solutions," *Colloid & Polymer Science*, vol. 286, no. 10, pp. 1173–1180, 2008.

[3] K. Bekkour, D. Sun-Waterhouse, and S. S. Wadhwa, "Rheological properties and cloud point of aqueous carboxymethyl cellulose dispersions as modified by high or low methoxyl pectin," *Food Research International*, vol. 66, pp. 247–256, 2014.

[4] I. H. Mondal, *Carboxymethyl Cellulose: Pharmaceutical and Industrial Applications*, Nova Science Publishers, Hauppauge, NY, USA, 2019.

[5] E. Grzadka, J. Matusiak, A. Bastrzyk, and I. Polowczyk, "CMC as a stabiliser of metal oxide suspensions," *Cellulose*, vol. 27, no. 4, pp. 2225–2236, 2020.

[6] J. Chen, H. Li, C. Fang, Y. Cheng, T. Tan, and H. Han, "Synthesis and structure of carboxymethylcellulose with a high degree of substitution derived from waste disposable paper cups," *Carbohydrate Polymers*, vol. 237, article 116040, 2020.

[7] M. Saqib, I. Khan, and S. Shafie, "Natural convection channel flow of CMC-based CNTs nanofluid," *European Physical Journal Plus*, vol. 133, no. 12, p. 549, 2018.

[8] A. R. Rahmati, O. A. Akbari, A. Marzban, D. Toghraie, R. Karimi, and F. Pourfattah, "Simultaneous investigations the effects of non-Newtonian nanofluid flow in different volume fractions of solid nanoparticles with slip and no-slip boundary conditions," *Thermal Science and Engineering Progress*, vol. 5, pp. 263–277, 2018.

[9] F. O. Akinpelu, R. M. Alabison, and O. A. Olaleye, "Thermophysical properties of nanoparticles in carboxylmethyl cellulose water mixture for heat enhancement applications," *IOP Conference Series Mater Science Engineering*, vol. 805, no. 1, article 012025, 2020.

[10] F. A. Alwawi, H. T. Alkasasbeh, A. M. Rashad, and R. A. Idris, "A Numerical approach for the heat transfer flow of Carboxymethyl cellulose-water based Casson nanofluid from a solid sphere generated by mixed convection under the influence of Lorentz force," *Mathematics*, vol. 8, no. 7, p. 1094, 2020.

[11] S. U. Choi and J. A. Eastman, *Enhancing Thermal Conductivity of Fluids with Nanoparticles; Technical Report*, Argonne National Lab, Argonne, IL, USA, 1995.

[12] J. Buongiorno, "Convective transport in nanofluids," *Journal of Heat Transfer*, vol. 128, no. 3, pp. 240–250, 2006.

[13] R. K. Tiwari and M. K. Das, "Heat transfer augmentation in a two-sided lid-driven differentially heated square cavity utilizing nanofluids," *International Journal of Heat and Mass Transfer*, vol. 50, no. 9-10, pp. 2002–2018, 2007.

[14] S. A. Devi and S. S. U. Devi, "Numerical investigation of hydromagnetic hybrid Cu – Al2O3/water nanofluid flow over a permeable stretching sheet with suction," *International Journal of Nonlinear Science Numerical Simulation*, vol. 17, no. 5, pp. 249–257, 2016.

[15] M. I. Afridi, M. Qasim, N. A. Khan, and M. Hamdani, "Heat transfer analysis of cu–Al2O3–water and cu– Al2O3–kerosene oil hybrid nanofluids in the presence of frictional heating: using 3-stage Lobatto IIIA formula," *Journal of Nanofluids*, vol. 8, no. 4, pp. 885–891, 2019.

[16] U. Farooq, M. Afridi, M. Qasim, and D. Lu, "Transpiration and viscous dissipation effects on entropy generation in hybrid nanofluid flow over a nonlinear radially stretching disk," *Entropy*, vol. 20, no. 9, p. 668, 2018.

[17] S. U. Devi and S. A. Devi, "Heat transfer enhancement of cu-Al2O3/water hybrid Nanofluid flow over a stretching sheet," *Journal of the Nigerian Mathematical Society*, vol. 36, pp. 419–433, 2017.

[18] S. S. U. Devi and S. P. A. Devi, "Numerical investigation of three-dimensional hybrid Cu–Al2O3/water nanofluid flow over a stretching sheet with effecting Lorentz force subject to Newtonian heating," *Canadian Journal of Physics*, vol. 94, no. 5, pp. 490–496, 2016.

[19] R. S. R. Gorla, S. Siddiqa, M. A. Mansour, A. M. Rashad, and T. Salah, "Heat source/sink effects on a hybrid nanofluid-filled porous cavity," *Journal of Thermophysics and Heat Transfer*, vol. 31, no. 4, pp. 847–857, 2017.

[20] J. Chamkha, I. V. Miroshnichenko, and M. A. Sheremet, "Numerical analysis of unsteady conjugate natural convection of hybrid water-based nanofluid in a semicircular cavity," *Journal of Thermal Science and Engineering Applications*, vol. 9, no. 4, article 41004, 2017.

[21] N. A. Zainal, R. Nazar, K. Naganthran, and I. Pop, "Unsteady three-dimensional MHD non-axisymmetric Homann stagnation point flow of a hybrid Nanofluid with stability analysis," *Mathematics*, vol. 8, no. 5, p. 784, 2020.

[22] K. Loganathan, K. Mohana, M. Mohanraj, P. Sakthivel, and S. Rajan, "Impact of third-grade nanofluid flow across a convective surface in the presence of inclined Lorentz force: an approach to entropy optimization," *Journal of Thermal Analysis and Calorimetry*, vol. 144, no. 5, pp. 1935–1947, 2021.

[23] M. Ramzan, A. Dawar, A. Saeed, P. Kumam, W. Watthayu, and W. Kumam, "Heat transfer analysis of the mixed convective flow of magnetohydrodynamic hybrid nanofluid past a stretching sheet with velocity and thermal slip conditions," *PLoS One*, vol. 16, no. 12, 2021.

[24] I. Ahmad, M. Faisal, Q. Zan-Ul-Abadin, T. Javed, and L. Karuppusamy, "Unsteady 3D heat transport in hybrid nanofluid containing brick shaped ceria and zinc-oxide nanocomposites with heat source/sink," *Nanocomposites*, vol. 8, no. 1, pp. 1–12, 2022.

[25] A. Dawar, E. Bonyah, S. Islam, A. Alshehri, and Z. Shah, "Theoretical analysis of Cu-H2O, Al2O3-H2O, and TiO2-H2O nanofluid flow past a rotating disk with velocity slip and convective conditions," *Journal of Nanomaterials*, vol. 2021, Article ID 5471813, 10 pages, 2021.

[26] S. Eswaramoorthi, S. Divya, M. Faisal, N. Namgyel, M. Faisal, and N. Namgyel, "Entropy and Heat Transfer Analysis for MHD Flow ofCu/Ag-Water-Based Nanofluid on a Heated 3D Plate with Nonlinear Radiation," *Mathematical Problems in Engineering*, vol. 2022, Article ID 7319988, 14 pages, 2022.

[27] A. Dawar, Z. Shah, A. Tassaddiq, P. Kumam, S. Islam, and W. Khan, "A convective flow of Williamson nanofluid through cone and wedge with non- isothermal and non-isosolutal conditions: a revised Buongiorno model," *Case Studies in Thermal Engineering*, vol. 24, article 100869, 2021.

[28] K. Loganathan, N. Alessa, and S. Kayikci, “Heat transfer analysis of 3-D viscoelastic nanofluid flow over a convectively heated porous Riga plate with Cattaneo-Christov double flux,” *Frontiers of Physics*, vol. 9, article 641645, 2021.

[29] A. Bejan, “Second-law analysis in heat transfer and thermal design,” *Advances in Heat Transfer*, vol. 15, pp. 1–58, 1982.

[30] M. Ijaz Khana, M. U. Hafeez, T. Hayat, M. Imran Khan, and A. Alsaedi, “Magneto rotating flow of hybrid nanofluid with entropy generation,” *Computer Methods and Programs in Biomedicine*, vol. 183, article 105093, 2020.

[31] S. Ahmad, S. Nadeem, and N. Ullah, “Entropy generation and temperature-dependent viscosity in the study of SWCNT–MWCNT hybrid nanofluid,” *Applied Nanoscience*, vol. 10, no. 12, pp. 5107–5119, 2020.

[32] A. S. Butt, M. N. Tufail, A. Ali, and A. Dar, “Theoretical investigation of entropy generation effects in nanofluid flow over an inclined stretching cylinder,” *International Journal of Exergy*, vol. 28, no. 2, pp. 126–157, 2019.

[33] M. M. Rashidi, S. Bagheri, E. Momoniat, and N. Freidoonimehr, “Entropy analysis of convective MHD flow of third grade non-Newtonian fluid over a stretching sheet,” *Ain Shams Engineering Journal*, vol. 8, no. 1, pp. 77–85, 2017.

[34] O. D. Makinde and A. S. Eegunjobi, “Entropy generation in a couple stress fluid flow through a vertical channel filled with saturated porous media,” *Entropy*, vol. 15, no. 12, pp. 4589–4606, 2013.

[35] Z. H. Khan, O. D. Makinde, R. Ahmad, and W. A. Khan, “Numerical study of unsteady MHD flow and entropy generation in a rotating permeable channel with slip and hall effects,” *Communications in Theoretical Physics*, vol. 70, no. 5, p. 641, 2018.

[36] M. I. Afridi, I. Tlili, M. Goodarzi, M. Osman, and N. A. Khan, “Irreversibility analysis of hybrid nanofluid flow over a thin needle with effects of energy dissipation,” *Symmetry.*, vol. 11, no. 5, p. 663, 2019.

[37] C. Srinivas Reddy, F. Ali, B. Mahanthesh, and K. Naikoti, “Irreversibility analysis of radiative heat transport of Williamson material over a lubricated surface with viscous heating and internal heat source,” *Heat Transfer*, vol. 51, pp. 395–412, 2022.

[38] M. M. Cross, “Rheology of non-Newtonian fluids: a new flow equation for pseudoplastic systems,” *Journal of Colloid Science*, vol. 20, no. 5, pp. 417–437, 1965.

[39] R. Ponalagusamy, R. T. Selvi, and A. K. Banerjee, “Mathematical model of pulsatile flow of non-Newtonian fluid in tubes of varying cross-sections and its implications to blood flow,” *Journal of Franklin Institue*, vol. 349, no. 5, pp. 1681–1698, 2012.

[40] A. R. Haghighi, N. Pirhadi, and M. Shahbazi Asl, “A Mathematical modeling for the study of blood flow as a cross fluid through a tapered artery,” *Journal of New Researches in Mathematics*, vol. 5, no. 20, pp. 15–30, 2019.

[41] M. Nazeer, “Numerical and perturbation solutions of cross flow of an Eyring-Powell fluid,” *SN Applied Science*, vol. 3, no. 2, pp. 1–11, 2021.

[42] Z. Sabir, A. Imran, M. Umar, M. Zeb, M. Shoaib, and M. A. Z. Raja, “A numerical approach for 2-D Sutterby fluid-flow bounded at a stagnation point with an inclined magnetic field and thermal radiation impacts,” *Thermal Science*, vol. 25, no. 3 Part A, pp. 1975–1987, 2021.

[43] L. Yao, A. Grishaev, G. Cornilescu, and A. Bax, “The impact of hydrogen bonding on amide 1H chemical shift anisotropy studied by cross-correlated relaxation and liquid crystal NMR spectroscopy,” *Journal of the American Chemical Society*, vol. 132, no. 31, pp. 10866–10875, 2010.

[44] M. I. Khan, T. Hayat, M. I. Khan, and A. Alsaedi, “Activation energy impact in nonlinear radiative stagnation point flow of Cross nanofluid,” *International Communication of Heat Mass Transfer*, vol. 91, pp. 216–224, 2018.

[45] C. S. Reddy and F. Ali, “Cattaneo–Christov double diffusion theory for MHD cross nanofluid flow towards a vertical stretching sheet with activation energy,” *International Journal of Ambient Energy*, pp. 1–10, 2021.

[46] S. Z. Abbas, W. A. Khan, H. Sun et al., “Mathematical modeling and analysis of Cross nanofluid flow subjected to entropy generation,” *Applied Nanoscience*, vol. 10, no. 8, pp. 3149–3160, 2020.

[47] M. Ali, W. A. Khan, M. Irfan, F. Sultan, M. Shahzed, and M. Khan, “Computational analysis of entropy generation for Cross-nanofluid flow,” *Applied Nanoscience*, vol. 10, no. 8, pp. 3045–3055, 2020.

[48] A. Wakif, “A novel numerical procedure for simulating steady MHD convective flows of radiative Casson fluids over a horizontal stretching sheet with irregular geometry under the combined influence of temperature-dependent viscosity and thermal conductivity,” *Mathematical Problems in Engineering*, vol. 2020, Article ID 1675350, 20 pages, 2020.

[49] F. Ali and A. Zaib, “Unsteady flow of an Eyring-Powell nanofluid near stagnation point past a convectively heated stretching sheet,” *Arab Journal of Basic and Applied Science*, vol. 26, no. 1, pp. 215–224, 2019.